

Close-slow analysis for head-on collision of two black holes in higher dimensions: Bowen-York initial data

Hiroataka Yoshino^(1,2), Tetsuya Shiromizu⁽³⁾, and Masaru Shibata⁽⁴⁾

⁽¹⁾ *Department of Physics, University of Alberta,
Edmonton, Alberta, Canada T6G 2G7*

⁽²⁾ *Graduate School of Science and Engineering,
Waseda University, Tokyo 169-8555, Japan*

⁽³⁾ *Department of Physics, Tokyo Institute of Technology, Tokyo 152-8551, Japan and*

⁽⁴⁾ *Graduate School of Arts and Sciences,
University of Tokyo, Komaba, Meguro, Tokyo 153-8902, Japan*

(Dated: October 23, 2006; revised November 28, 2006; published December 20, 2006)

Abstract

Scenarios of large extra dimensions have enhanced the importance for the study of black holes in higher dimensions. In this paper, we analyze an axisymmetric system of two black holes. Specifically, the Bowen-York method is generalized for higher dimensions in order to calculate the initial data for head-on collision of two equal-mass black holes. Then, the initial data are evolved adopting the close-slow approximation to study gravitational waves emitted during the collision. We derive an empirical formula for radiation efficiency, which depends weakly on the dimensionality. Possible implications of our results for the black hole formation in particle colliders are discussed.

PACS numbers: 04.70.-s, 04.30.Db, 04.50.+h, 11.25.-w

I. INTRODUCTION

Motivated by scenarios of large extra dimensions [1, 2, 3], the study of black holes in higher dimensions has attracted attention. In these scenarios, extradimensional effects play an important role for the properties of black holes with radius smaller than the size of extra dimensions. An interesting phenomena is mini-black hole production in planned accelerators. If the Planck energy is of $O(\text{TeV})$ as suggested in scenarios of [1, 2], phenomena associated with quantum gravity will be observed at the CERN Large Hadron Collider (LHC) through black hole production [4, 5]. At the LHC, the produced black hole is expected to settle down to a higher-dimensional Kerr black hole after emission of gravitational waves. The formed black hole will be subsequently evaporated by the Hawking radiation, for which high-energy particles are emitted and may be detected. To know the parameters of the formed Kerr black hole which determines the feature of the Hawking radiation observed, studies for gravitational radiation are an important issue.

In this paper, we study axisymmetric collision of two black holes in higher dimensions as a first step for the investigations on the black holes formed in particle colliders ¹. This is an extension of our previous study [6] of the higher-dimensional Brill-Lindquist initial data and its temporal evolution by the close-limit approximation. In four dimensions, there is the well-known Bowen-York method [7] for generating initial data of several moving black holes. We generalize this method for higher dimensions. Similarly to the four-dimensional case, the conformally transformed extrinsic curvature is given analytically and the conformal factor should be calculated numerically. We perform numerical calculation for the conformal factor in the case of the head-on collision of two equal-mass black holes and then determine the location of apparent horizon (AH) that encloses two black holes (the common AH). We clarify the parameter space for common AH formation.

Then, the initial data is evolved adopting the close-slow approximation. In this approximation, the distance between two black holes and the linear momentum of each black hole are regarded as small parameters compared to the black hole size and the gravitational mass of the system, respectively. In this case, the system may be considered to be a perturbed

¹ Here, the incoming black holes are regarded as substitutes for the incoming particles. We do not consider the collision of produced black holes, since they are evaporated within the time scale of 10^{-27} s but only one black hole is produced per 1 s.

single Schwarzschild black hole. In the four-dimensional case, the results in the close-slow approximation agree with those in the fully nonlinear analysis (see [8, 9] and references in [6]), and hence, it is natural to expect that this is also the case in the higher-dimensional case. We provide a formula for the radiation efficiency (i.e., the ratio of the radiated energy to the system energy) and discuss their dependence on the dimensionality.

The purpose of this paper is twofold. One is to present a formulation for providing the initial condition of colliding black holes in higher dimensions. Gravitational waves at the collision of two black holes are accurately computed only by a fully nonlinear numerical relativity simulation. Although such a simulation has not been done yet for higher-dimensional space-time, several groups have developed robust techniques for numerically computing merger of binary black holes in four dimensions [10]. The methods used in four dimensions can be applied for higher-dimensional problems and hence, the simulation will be done in the near future. For such future simulations, a method for providing initial condition we present here will be useful.

The second purpose is to approximately evaluate gravitational radiation in the collision of two black holes in the higher-dimensional case. Since we adopt a linear perturbative method, a reliable result is derived only for a small parameter space. However, our result for such parameters will be useful for calibrating fully nonlinear results in the near future.

This paper is organized as follows. In the next section, we derive a generalized Bowen-York formulation [7] for higher-dimensional space. Applying the formulation, we construct the initial data for head-on collision of two equal-mass black holes in Sec. III. The ADM mass and the common AH are analyzed. In Sec. IV, we evolve the initial data adopting the close-slow approximation. The master variable of the linear perturbation around a D -dimensional Schwarzschild black hole is calculated numerically and the formula for radiation efficiency is derived. The radiation efficiency is shown to depend weakly on the dimensionality. Sec. V is devoted to a discussion on possible implication of our results for the radiation efficiency in the particle collision. In Appendix A, we present some solutions of the extrinsic curvature in the generalized Bowen-York formulation that were not introduced in Sec. II. In Appendix B, the method for imposing the initial condition for the master variable is explained.

II. HIGHER-DIMENSIONAL BOWEN-YORK METHOD

In this section we generalize the Bowen-York formulation for higher dimension space and present a method for generating initial condition of N black holes with linear momenta.

A. Formulation

Let $\Sigma(h_{\mu\nu}, K_{\mu\nu})$ be a $(D - 1)$ -dimensional spacelike hypersurface Σ with the metric $h_{\mu\nu}$ and the extrinsic curvature $K_{\mu\nu}$ in a D -dimensional spacetime. We introduce a number $n = D - 2$. The Hamiltonian and momentum constraints are

$${}^{(n+1)}R - K^{\mu\nu}K_{\mu\nu} + K^2 = 0, \quad (1)$$

$$\nabla^\mu(K_{\mu\nu} - h_{\mu\nu}K) = 0, \quad (2)$$

where ${}^{(n+1)}R$ denotes the Ricci scalar of Σ and ∇^μ is the covariant derivative with respect to $h_{\mu\nu}$. Introducing $\widehat{h}_{\mu\nu}$ defined by

$$\widehat{h}_{\mu\nu} = \Psi^{-4/(n-1)}h_{\mu\nu}, \quad (3)$$

the Hamiltonian and momentum constraints are rewritten as

$$\widehat{\nabla}^2\Psi = \frac{n-1}{4n} \left[{}^{(n+1)}\widehat{R}\Psi - \Psi^{(n+3)/(n-1)}(K^{\mu\nu}K_{\mu\nu} - K^2) \right], \quad (4)$$

$$\widehat{\nabla}_\nu(\Psi^{2(n+1)/(n-1)}K_\mu^\nu) - \Psi^{2(n+1)/(n-1)}\widehat{\nabla}_\mu K - \frac{2}{n-1}K\Psi^{(n+3)/(n-1)}\widehat{\nabla}_\mu\Psi = 0, \quad (5)$$

where ${}^{(n+1)}\widehat{R}$ and $\widehat{\nabla}_\mu$ denote the Ricci scalar and the covariant derivative with respect to $\widehat{h}_{\mu\nu}$, respectively. Here raising and lowering the index are done with $h_{\mu\nu}$.

In the following, we assume the conformal flatness on Σ , $\widehat{h}_{\mu\nu} = \delta_{\mu\nu}$, and impose the maximal slicing condition, $K = 0$. A weighted extrinsic curvature is defined by $\widehat{K}_{\mu\nu} = \Psi^2 K_{\mu\nu}$ and hereafter its index is raised and lowered by $\delta_{\mu\nu}$ (i.e., $\widehat{K}_\nu^\mu = \Psi^{2(n+1)/(n-1)}K_\nu^\mu$ and $\widehat{K}^{\mu\nu} = \Psi^{2(n+3)/(n-1)}K^{\mu\nu}$). Then the Hamiltonian and momentum constraints become

$$\nabla_{\text{f}}^2\Psi = -\frac{n-1}{4n}\widehat{K}_{\mu\nu}\widehat{K}^{\mu\nu}\Psi^{-(3n+1)/(n-1)}, \quad (6)$$

$$\partial^\mu\widehat{K}_{\mu\nu} = 0, \quad (7)$$

where ∂_μ denotes the ordinary derivative with respect to the Cartesian coordinate (x^μ) and $\nabla_{\mathfrak{f}}^2 = \partial^\mu \partial_\mu$. Following Bowen and York [7], we assume that $\widehat{K}_{\mu\nu}$ does not have the tensor mode and thus takes the following form:

$$\widehat{K}_{\mu\nu} = \partial_\mu W_\nu + \partial_\nu W_\mu - \frac{2}{n+1} \delta_{\mu\nu} \partial_\rho W^\rho. \quad (8)$$

Substituting this formula into the momentum constraint (7), we obtain

$$\nabla_{\mathfrak{f}}^2 W_\mu + \frac{n-1}{n+1} \partial_\mu \partial_\nu W^\nu = 0. \quad (9)$$

Introducing auxiliary functions B_μ and χ , we decompose W_μ as

$$W_\mu = \frac{3n+1}{n-1} B_\mu - (\partial_\mu \chi + x^\nu \partial_\mu B_\nu). \quad (10)$$

Then the equation becomes

$$0 = \frac{3n+1}{n-1} \nabla_{\mathfrak{f}}^2 B_\mu - \frac{2n}{n+1} \partial_\mu \nabla_{\mathfrak{f}}^2 \chi - x^\nu \partial_\mu \nabla_{\mathfrak{f}}^2 B_\nu - \frac{n-1}{n+1} \partial_\mu (x^\nu \nabla_{\mathfrak{f}}^2 B_\nu). \quad (11)$$

Hence the momentum constraint is satisfied if

$$\nabla_{\mathfrak{f}}^2 B_\mu = 0, \quad (12)$$

$$\nabla_{\mathfrak{f}}^2 \chi = 0. \quad (13)$$

Since the solutions of Eqs. (12) and (13) are analytically given, solutions for \widehat{K}_{ab} are easily provided.

B. N -black-hole solutions

To give linear momenta of black holes, we choose the solution

$$B_\mu = -\frac{2\pi G P_\mu}{n\Omega_n R^{n-1}}, \quad \chi = 0, \quad (14)$$

where P_μ is a constant vector, G the gravitational constant, Ω_n the n -dimensional area of a unit sphere, and $R = |x^\mu|$. Then, we obtain

$$\widehat{K}_{\mu\nu} = \frac{4\pi(n+1)G}{n\Omega_n R^n} \{P_\mu n_\nu + P_\nu n_\mu + P_\rho n^\rho [(n-1)n_\mu n_\nu - \delta_{\mu\nu}]\}, \quad (15)$$

where $n^\mu = x^\mu/R$. This solution provides the extrinsic curvature for one boosted black hole located at $R = 0$. Actually, P_μ agrees with the ADM momentum:

$$P_\mu = \frac{1}{8\pi G} \int_{R \rightarrow \infty} (K_{\mu\nu} n^\nu - K n_\mu) dS. \quad (16)$$

Since the momentum constraint (7) is a linear equation, we can superpose N solutions. Denoting the locations of N black holes as $x_a^\mu (a = 1, \dots, N)$, a solution of the extrinsic curvature is written as

$$\widehat{K}_{\mu\nu} = \sum_{a=1}^N \frac{4\pi(n+1)G}{n\Omega_n R_a^n} \{ (P_a)_\mu (n_a)_\nu + (P_a)_\nu (n_a)_\mu + (P_a)_\rho (n_a)^\rho [(n-1)(n_a)_\mu (n_a)_\nu - \delta_{\mu\nu}] \}, \quad (17)$$

where $R_a = |x^\mu - x_a^\mu|$, $n_a^\mu = (x^\mu - x_a^\mu)/R_a$, and $(P_a)_\mu$ denotes the momentum of the a th black hole.

The conformal factor Ψ is obtained by solving the Hamiltonian constraint (6). Following [11], we assume that Ψ has the following form

$$\Psi = \Psi_{\text{BL}} + \psi, \quad (18)$$

where

$$\Psi_{\text{BL}} \equiv 1 + \frac{4\pi G}{n\Omega_n} \sum_{a=1}^N \frac{M_a}{R_a^{n-1}} \quad (19)$$

and M_a denotes the mass parameter of a th black hole. Then, the equation for ψ becomes

$$\nabla_{\text{f}}^2 \psi = -\frac{(n-1)}{4n} \widehat{K}_{\mu\nu} \widehat{K}^{\mu\nu} (\Psi_{\text{BL}} + \psi)^{-(3n+1)/(n-1)}. \quad (20)$$

The solution in this procedure represents the so-called ‘‘puncture’’ space with N Einstein-Rosen bridges and $N + 1$ asymptotically flat regions (say, one upper sheet and N lower sheets).

Since the right hand side of Eq. (20) behaves like $O(R_a^{n-1})$ for $R_a \rightarrow 0$, there is a regular solution for ψ , which can be solved numerically (this fact was first pointed out in [11] for the four-dimensional case). The ADM mass M_{ADM} is given by

$$M_{\text{ADM}} = \frac{-n}{4\pi(n-1)G} \int_{R \rightarrow \infty} \partial_\mu \Psi n^\mu dS. \quad (21)$$

Using the Gauss law, we find

$$M_{\text{ADM}} = \sum_{a=1}^N M_a + \frac{1}{16\pi G} \int_{\Sigma} \widehat{K}^{\mu\nu} \widehat{K}_{\mu\nu} \Psi^{-(3n+1)/(n-1)} d^{n+1}x. \quad (22)$$

The first and second terms could be interpreted as the sum of the mass of N black holes and the kinetic energy of the black holes, respectively.

III. INITIAL DATA FOR HEAD-ON COLLISION OF TWO BLACK HOLES

In this section, we present initial data of the axisymmetric two-black-hole system following the formalism described in the previous section.

A. Calculating conformal factor

We introduce the Cartesian coordinate (z, x_k) , $(k = 1, \dots, n)$ for $(n+1)$ -dimensional space and write the solution of $\widehat{K}_{\mu\nu}$ as

$$\widehat{K}_{\mu\nu} = \widehat{K}_{\mu\nu}^{(+)} + \widehat{K}_{\mu\nu}^{(-)}, \quad (23)$$

where two black holes (\pm) are located at $(z, x_k) = (\pm z_0, 0)$ and have momenta $P_\mu^{(\pm)} = (\mp P, 0)$. We assume that the two black holes have the same mass $M_+ = M_- = M_0/2$.

The gravitational radius of a black hole of mass M_0 is defined by

$$r_h(M_0) = \left(\frac{16\pi G M_0}{n\Omega_n} \right)^{1/(n-1)}. \quad (24)$$

In the case $z_0 = 0$, the common apparent horizon (AH) that encloses two black holes is located at $R = R_h(M_0)$ where

$$R_h(M_0) = 4^{-1/(n-1)} r_h(M_0). \quad (25)$$

Using $R_h(M_0)$ the conformal factor in the puncture framework [11] is given by

$$\Psi = \Psi_{\text{BL}} + \psi, \quad (26)$$

where

$$\Psi_{\text{BL}} = 1 + \frac{1}{2} [R_h(M_0)]^{n-1} \left(\frac{1}{R_+^{n-1}} + \frac{1}{R_-^{n-1}} \right). \quad (27)$$

For a numerical solution of ψ , we introduce the cylindrical coordinate (z, ρ) where $\rho = \sqrt{\sum_{k=1}^n x_k^2}$. In this coordinate, the equation for ψ becomes

$$\psi_{,\rho\rho} + \psi_{,zz} + \frac{(n-1)}{\rho} \psi_{,\rho} + \frac{n+1}{4n} \widehat{K}_{\mu\nu} \widehat{K}^{\mu\nu} \Psi^{-(3n+1)/(n-1)} = 0. \quad (28)$$

Since the system is axisymmetric and equatorial-plane symmetric, it is sufficient to solve the equation for the domain $0 \leq \rho \leq \rho_{\text{max}}$ and $0 \leq z \leq z_{\text{max}}$ with the boundary conditions

$\psi_{,\rho} = 0$ at the z -axis and $\psi_{,z} = 0$ at the equatorial plane. For $R \rightarrow \infty$, ψ asymptotically behaves as

$$\psi \simeq \frac{4\pi G(M_{\text{ADM}} - M_0)}{n\Omega_n R^{n-1}} + O(1/R^n). \quad (29)$$

Thus, we impose the so-called Robin condition, $\psi_{,R} = -(n-1)\psi/R$, at the outer boundary. In the cylindrical coordinate, it is rewritten as

$$\psi_{,\rho\rho} + \psi_{,zz} = -(n-1)\psi. \quad (30)$$

We put the outer boundary at $\rho_{\text{max}} = z_{\text{max}} = 5R_h(M_0)$ and solve the equation for ψ using a finite difference method with the grid number (101×101) . Numerical computation was carried out for the parameter space $0 \leq z_0/R_h(M_0) \leq 1$ and $0 \leq P/M_0 \leq 1$ with the 0.1 interval or the 0.01 interval.

There are two sources for numerical error of the conformal factor: One is associated with the finiteness of the grid spacing and the other with the finiteness of the outer boundary location. To evaluate the numerical error by the grid spacing, we took reference data with sufficiently large grid number (401×401 grids) and evaluated following three characteristic numerical error values:

$$\begin{aligned} \epsilon_1 &= \frac{\sum_N |\psi_N - \psi_N^{(\text{ref})}|}{\sum_N |\psi_N^{(\text{ref})}|}, \\ \epsilon_2 &= \max \left(\left| \Psi_N - \Psi_N^{(\text{ref})} \right| / \left| \Psi_N^{(\text{ref})} \right| \right), \\ \epsilon_3 &= \max \left(\left| \psi_N - \psi_N^{(\text{ref})} \right| / \left| \psi_N^{(\text{ref})} \right| \right), \end{aligned} \quad (31)$$

where N stands for the label of the grids. Changing the grid spacing, we confirm that ϵ_1 decreases with improving the grid resolution at second order. All the three error estimates were found to be small. With our standard choice, ϵ_2 is 0.005–0.2% for $D = 4$ –11. Computation was also performed changing the location of the outer boundaries from $\rho_{\text{max}} = z_{\text{max}} = 5R_h(M_0)$ to $20R_h(M_0)$ and the numerical solution converges with increasing the radius of the outer boundaries. In this case, ϵ_3 is found to be relatively large, about 9–17% for $D = 4$ –11. Such large differences occur at outer boundaries and come from the fact that the Robin condition is an approximate boundary condition. However, because ψ is small at the outer boundary, the error of the conformal factor Ψ is small. In fact, we found that ϵ_2 is about 0.3% for $D = 4$ and becomes smaller as D is increased (less than 0.01% in

the case $D = 11$). The error ϵ_1 is smaller than ϵ_3 by a factor for $D = 4$ and is comparable to ϵ_2 for $D = 11$. Because Ψ is used in the calculations of the ADM mass or the AH, the error for these calculations is expected to have the order of ϵ_2 . Hence, we consider that sufficient accuracy is obtained in our calculation.

Figure 1 shows the contours of M_{ADM}/M_0 on the $(z_0/R_h(M_0), P/M_0)$ -plane for $D = 4$ –11. The difference between M_{ADM} and M_0 indicates the strength of nonlinearity due to the right hand side of the Hamiltonian constraint (6). We find that the nonlinearity of the system becomes large as D is increased for fixed values of $z_0/R_h(M_0)$ and P/M_0 .

B. Common apparent horizon

A common AH that covers two black holes is searched for introducing the spherical coordinate (R, θ) by $R = \sqrt{\rho^2 + z^2}$ and $\tan \theta = z/\rho$ and assuming that the location is denoted by $R = h(\theta)$. Then the equation for the AH is given by

$$\nabla_\mu s^\mu - K + K_{\mu\nu} s^\mu s^\nu = 0, \quad (32)$$

where s^μ is the unit normal to the surface:

$$s^\mu = \frac{\Psi^{-2/(n-1)}}{\sqrt{1 + h_{,\theta}^2/R^2}} (1, -h_{,\theta}/R^2). \quad (33)$$

Then, the equation for the AH reduces to an ordinary differential equation for $h(\theta)$:

$$h_{,\theta\theta} - n \left(\frac{2}{n-1} \frac{\Psi_{,R}}{\Psi} + \frac{1}{h} \right) (h^2 + h_{,\theta}^2) - \frac{h_{,\theta}^2}{h} + \left(\frac{2n}{n-1} \frac{\Psi_{,\theta}}{\Psi} + (n-1) \cot \theta \right) h_{,\theta} \left(1 + \frac{h_{,\theta}^2}{h^2} \right) - \Psi^{-2n/(n-1)} h \sqrt{h^2 + h_{,\theta}^2} \left(\widehat{K}_{RR} - 2\widehat{K}_{R\theta} \frac{h_{,\theta}}{h^2} + \widehat{K}_{\theta\theta} \frac{h_{,\theta}^2}{h^4} \right) = 0. \quad (34)$$

This equation is solved under the boundary conditions $h_{,\theta} = 0$ at $\theta = 0$ and $\pi/2$.

Figure 2 shows the critical line for the common AH formation. Irrespective of the dimensionality, the common AH is formed if $z_0/R_h(M_0)$ is sufficiently small. It is interesting to point out that, for $D = 4$, the AH formation is more subject for larger values of P while for $D \geq 5$, the presence of P tends to prevent formation of the common AH. This might seem strange because the kinetic energy is naturally expected to help the AH formation. In order to obtain a corroboration for this result, we direct attention to the AH (denoted by $R = \widehat{h}(\theta)$) at the critical separation $z_0 = z_0^{(\text{crit})}$ in the case $P = 0$. Then we add small

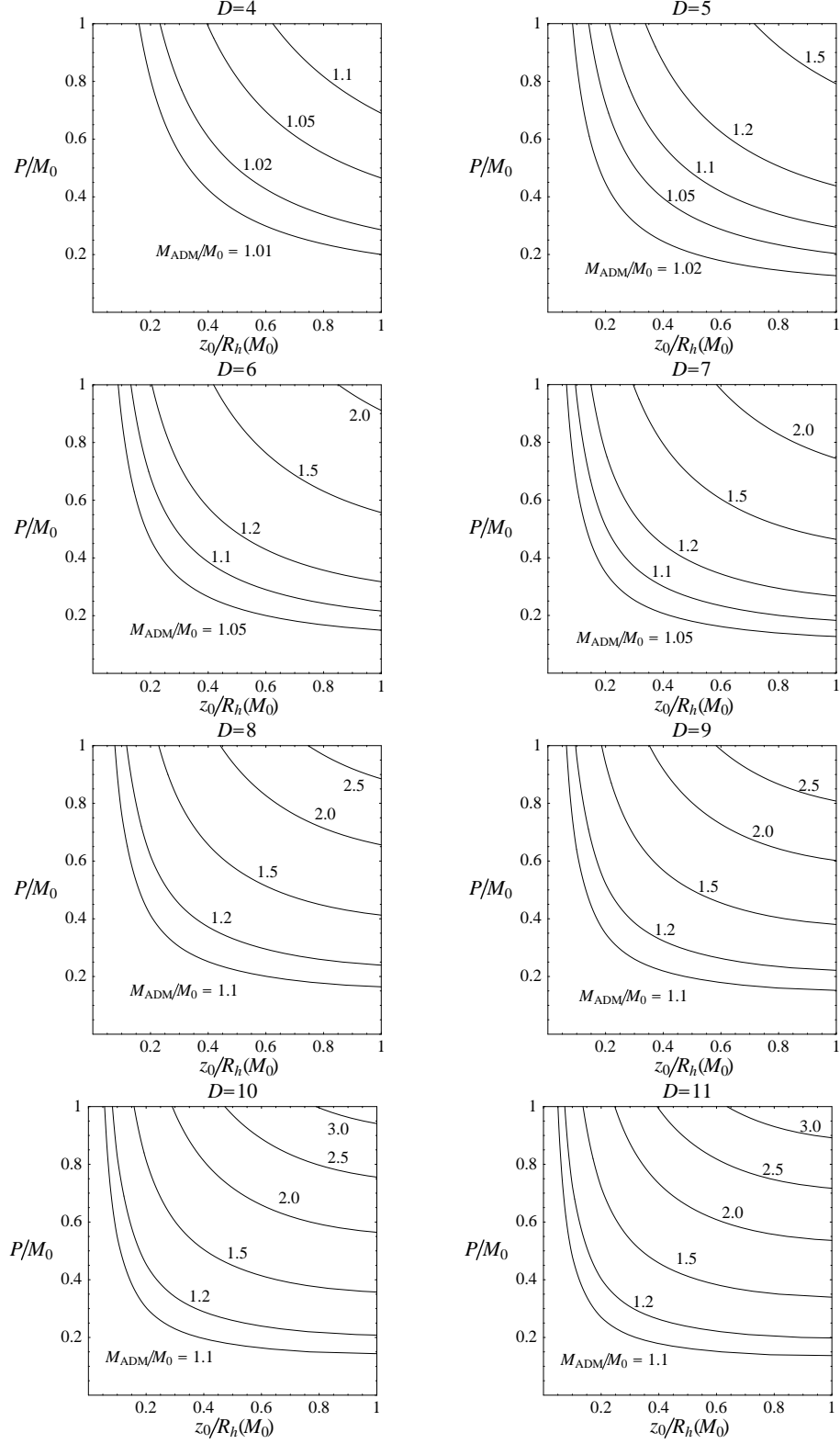


FIG. 1: The contour line for M_{ADM}/M_0 on the $(z_0/R_h(M_0), P/M_0)$ -plane.

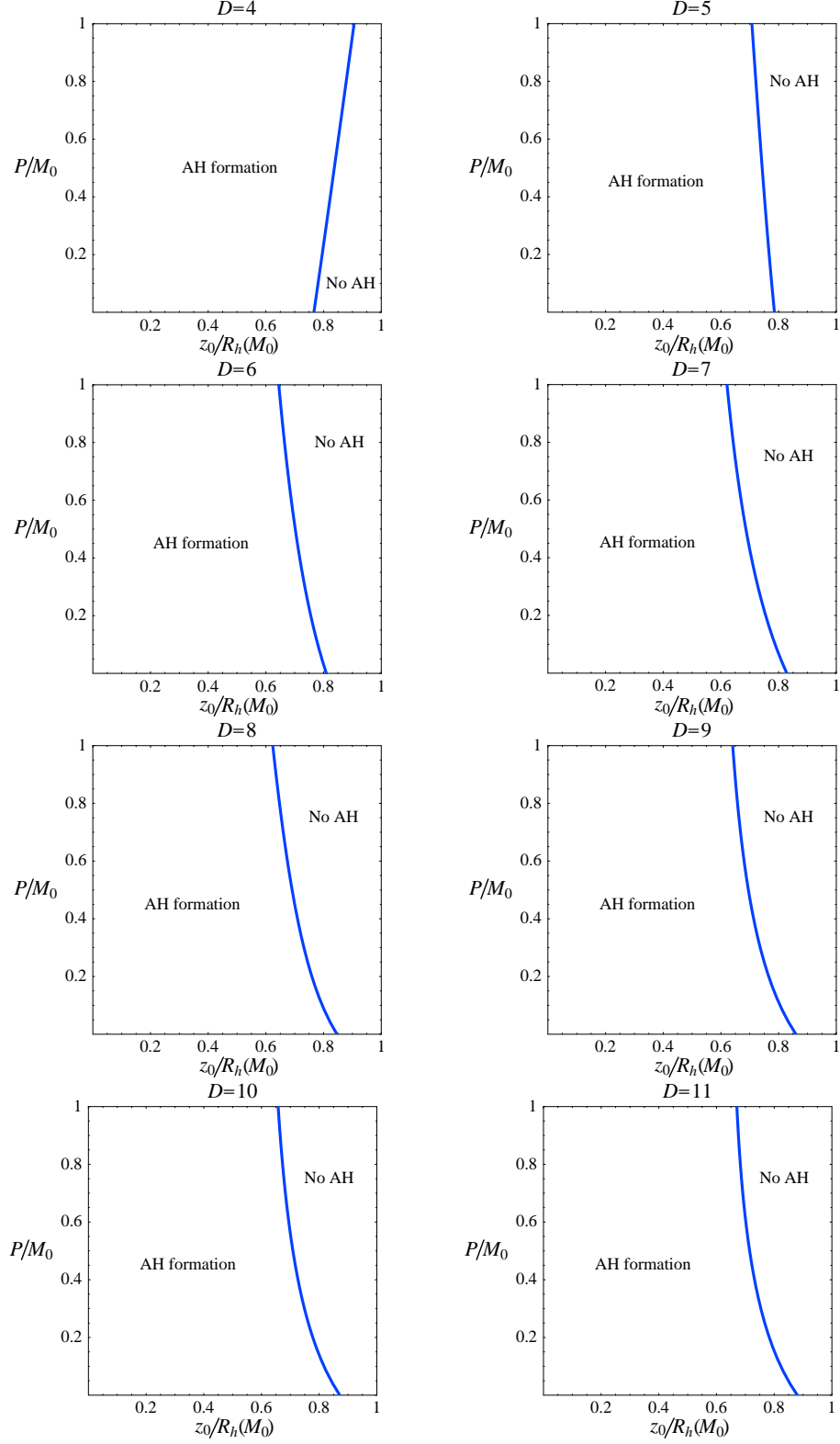


FIG. 2: The critical line for the common AH formation on the $(z_0/R_h(M_0), P/M_0)$ -plane.

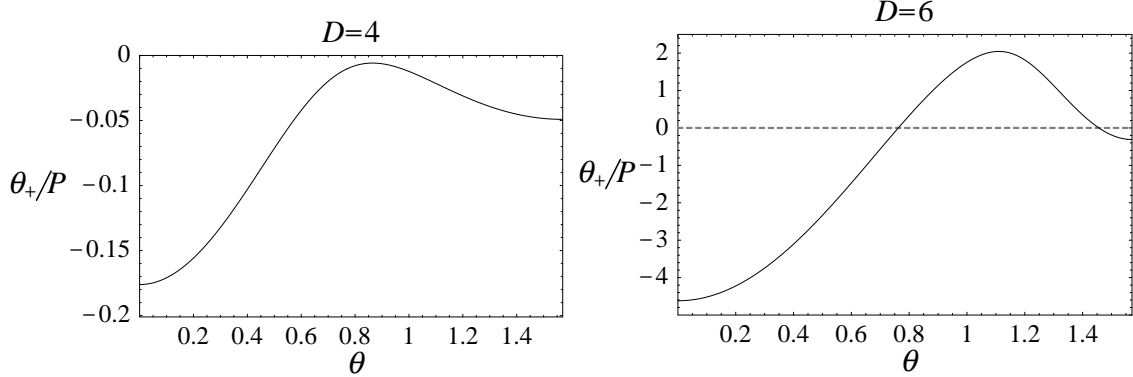


FIG. 3: The expansion θ_+ of a minimal surface in the $P \ll M_0$ case at the critical separation $z_0 = z_0^{(\text{crit})}$. The cases $D = 4$ (left) and 6 (right) are shown. In the case $D = 4$, θ_+ is negative for all θ and the minimal surface is a trapped surface. But in the case $D = 6$, there is a region of θ where θ_+ becomes positive, which means that the minimal surface is not a trapped surface.

$P \ll M_0$ without changing the value of z_0 . Because the change in the conformal factor is $O(P^2/M_0^2)$ and can be ignored, the surface $R = \hat{h}(\theta)$ is interpreted as a minimal surface on which $\nabla_\mu s^\mu = 0$ holds. Now let us consider the expansion on this minimal surface which is given by $\theta_+ = K_{\mu\nu} s^\mu s^\nu$. Figure 3 shows the behavior of θ_+/P in the four- and six-dimensional cases. In the case $D = 4$, we find that θ_+ is negative and thus the minimal surface is a trapped surface. This guarantees the existence of an AH outside of the minimal surface. Hence the motion helps AH formation in the four-dimensional case. On the other hand, in the case $D = 6$, θ_+ becomes positive on some part of the minimal surface. The similar behavior was found for all $5 \leq D \leq 11$. Therefore, the minimal surface is not a trapped surface and the motion does not necessarily help the AH formation in the higher-dimensional cases. We found numerically that the term $K_{\theta\theta} s^\theta s^\theta$ mainly contributes to the positivity of θ_+ . This is because for high D , the AH at the critical separation is hourglass shaped in the neighborhood of the equatorial plane and the value of $\hat{h}_{,\theta}$ is quite large around $\theta \simeq 1$. It enhances the value of $K_{\theta\theta} s^\theta s^\theta$ which is proportional to $\hat{h}_{,\theta}^2/\hat{h}^4$.

The AH mass M_{AH} is determined by the AH area A_{AH} as

$$M_{\text{AH}} = \frac{n\Omega_n}{16\pi G} \left(\frac{A_{\text{AH}}}{\Omega_n} \right)^{1/n}. \quad (35)$$

The area theorem of black hole constrains that the AH mass never decrease ². Thus, the

² Since the proof of the area theorem is not sensitive to the spacetime dimension, it holds also in the current

TABLE I: The values of $1 - M_{\text{AH}}/M_{\text{ADM}}$ evaluated on the AH critical line for $P/M_0 = 0.0, 0.5, 1.0$. The unit is %.

D	4	5	6	7	8	9	10	11
$P/M_0 = 0.0$	1.2	3.6	5.8	7.2	7.7	7.7	7.4	6.9
$P/M_0 = 0.5$	2.8	9.0	12	14	16	17	18	19
$P/M_0 = 1.0$	5.5	15	19	21	22	24	25	26

AH mass provides the lower bound on the black hole mass of the final state. In other words, the quantity $M_{\text{ADM}} - M_{\text{AH}}$ is the upper bound on gravitational radiation energy in the collision process. Table I shows the value of $1 - M_{\text{AH}}/M_{\text{ADM}}$ on the AH critical line for $P/M_0 = 0, 0.5, 1.0$. As the value of D increases, $1 - M_{\text{AH}}/M_{\text{ADM}}$ becomes large for fixed values of $P/M_0 = 0.5$ and 1.0 on the AH critical line. The area theorem provides a stricter condition for smaller value of D .

IV. CLOSE-SLOW ANALYSIS

Next we compute gravitational waves in the head-on collision of two black holes adopting the close-slow approximation. In this approximation, we assume that $z_0 \ll r_h(M_0)$, $P \ll M_0$, and $z_0/r_h(M_0) \sim P/M_0$, and evaluate gravitational wave energy up to order of $(z_0/r_h(M_0))^2$ using a linear perturbative approach. In the following, the gravitational radius of the system $r_h(M_0)$ is used as the unit of the length [i.e., $r_h(M_0) = 1$] unless specified.

A. Close-slow form of the initial data

Since we analyze gravitational waves in the Regge-Wheeler type method, $\widehat{K}_{\mu\nu}^{(\pm)}$ in the spherical-polar coordinate (R, θ, ϕ_*) , ($\phi_* = \phi_1, \dots, \phi_{n-1}$), should be derived:

$$\frac{4M_0}{(n+1)P} \widehat{K}_R^{R(\pm)} = \frac{\mp 2}{R_{\pm}^{n+1}} \cos \theta (R \mp z_0 \cos \theta) + \frac{z_0 \mp R \cos \theta}{R_{\pm}^{n+3}} [(n-1)(R \mp z_0 \cos \theta)^2 - R_{\pm}^2], \quad (36)$$

system as long as naked singularities do not exist.

$$\frac{4M_0}{(n+1)P} \frac{\widehat{K}_{R\theta}^{(\pm)}}{R} = \frac{\pm 1}{R_{\pm}^{n+1}} \sin \theta (R \mp 2z_0 \cos \theta) + \frac{z_0 \mp R \cos \theta}{R_{\pm}^{n+3}} [\pm(n-1)z_0 \sin \theta (R \mp z_0 \cos \theta)], \quad (37)$$

$$\frac{4M_0}{(n+1)P} \widehat{K}_{\theta}^{\theta(\pm)} = \frac{2}{R_{\pm}^{n+1}} z_0 \sin^2 \theta + \frac{z_0 \mp R \cos \theta}{R_{\pm}^{n+3}} [(n-1)z_0^2 \sin^2 \theta - R_{\pm}^2], \quad (38)$$

and

$$\frac{4M_0}{(n+1)P} \widehat{K}_{\phi_*}^{\phi_*(\pm)} = -\frac{z_0 \mp R \cos \theta}{R_{\pm}^{n+1}}. \quad (39)$$

For $z_0 \ll 1$, $K_{\mu\nu} = K_{\mu\nu}^{(+)} + K_{\mu\nu}^{(-)}$ is expanded as

$$\widehat{K}_R^R = (z_0 P/M_0) \frac{n+1}{2} [n-2 - (n^2+n-2) \cos^2 \theta] R^{-(n+1)} + O(z_0^2 P/M_0), \quad (40)$$

$$\widehat{K}_{\theta}^{\theta} = (z_0 P/M_0) \frac{n+1}{2} [(n-1) \cos^2 \theta + 1] R^{-(n+1)} + O(z_0^2 P/M_0), \quad (41)$$

$$\widehat{K}_{\phi_*}^{\phi_*} = (z_0 P/M_0) \frac{n+1}{2} [(n+1) \cos^2 \theta - 1] R^{-(n+1)} + O(z_0^2 P/M_0), \quad (42)$$

and $\widehat{K}_{R\theta} = O(z_0^3 P/M_0)$. The leading-order term of \widehat{K}_{ab} is found to be $O(z_0 P/M_0)$ and hence the right hand side of the Hamiltonian constraint (6) is of order $O(z_0^2 P^2/M_0^2)$. In the close-slow approximation adopted here, such terms are higher order and we ignore them. Thus, $\psi = 0$ and $M_{\text{ADM}} = M_0$ in this approximation.

As a result, the conformal factor is given by the Brill-Lindquist one:

$$\Psi \simeq \Psi_{\text{BL}} = 1 + \frac{1}{8} \left(\frac{1}{R_+^{n-1}} + \frac{1}{R_-^{n-1}} \right). \quad (43)$$

By transforming from the isotropic coordinate to the Schwarzschild-like coordinate

$$r = R\Psi_0^{2/(n-1)}, \quad \Psi_0 = 1 + \frac{1}{4R^{n-1}}, \quad (44)$$

we find that the system is regarded as a perturbed Schwarzschild black hole

$$ds^2 \simeq \left(\frac{\Psi_{\text{BL}}}{\Psi_0} \right)^{4/(n-1)} \left[\frac{dr^2}{f(r)} + r^2 (d\theta^2 + \sin^2 \theta d\Omega_{n-1}^2) \right], \quad f(r) = 1 - \frac{1}{r^{n-1}}, \quad (45)$$

$$\left(\frac{\Psi_{\text{BL}}}{\Psi_0} \right)^{4/(n-1)} = 1 + \frac{1/(n-1)R^{n-1}}{1 + 1/4R^{n-1}} \left(\frac{z_0}{R} \right)^2 C_2^{[(n-1)/2]}(\cos \theta) + O(z_0^4), \quad (46)$$

where $C_{\ell}^{[\lambda]}$ denotes the Gegenbauer polynomials defined by the generating function

$$(1 - 2xt + t^2)^{-\lambda} = \sum_{\ell=0}^{\infty} C_{\ell}^{[\lambda]}(x) t^{\ell}. \quad (47)$$

Note that the metric (45) with (46) is the same as that in our previous analysis of the time-symmetric initial data [6]. However, the time-asymmetry is present because of the presence of nonzero $\widehat{K}_{\mu\nu}$.

As found above, the order of the perturbation of the initial metric is $O(z_0^2)$ and of the extrinsic curvature is $O(z_0 P/M_0)$. In the following, we consider the situation where both z_0 and P/M_0 have the same order. Under this condition, we can evolve the system using a standard perturbation method in the Schwarzschild spacetime. From Eqs. (40)–(42), (45), and (46), the leading order of the perturbation contains only the $\ell = 2$ mode.

B. Time evolution by the master equation

The gauge-invariant method for the perturbation around the Schwarzschild black hole was developed by Kodama and Ishibashi [12]. They derived a master equation for a variable Φ , which is related to the gauge-invariant quantities of the perturbation, as

$$\frac{\partial^2 \Phi}{\partial t^2} - \frac{\partial^2 \Phi}{\partial r_*^2} + V_S \Phi = 0, \quad (48)$$

where

$$V_S(r) = \frac{f(r)Q(r)}{16r^2 H^2(r)}, \quad (49)$$

and

$$H(r) = m + (1/2)n(n+1)x, \quad x = 1/r^{n-1}, \quad (50)$$

$$m = k^2 - n, \quad k^2 = \ell(\ell + n - 1), \quad (51)$$

$$Q(r) = n^4(n+1)^2 x^3 + n(n+1) [4(2n^2 - 3n + 4)m + n(n-2)(n-4)(n+1)] x^2 - 12n [(n-4)m + n(n+1)(n-2)] mx + 16m^3 + 4n(n+2)m^2. \quad (52)$$

r_* denotes the tortoise coordinate defined by

$$r_* = \int \frac{dr}{f(r)}. \quad (53)$$

Initial values of Φ and $\dot{\Phi}$ (a dot denotes the time derivative hereafter) are related to the metric perturbation and \widehat{K}_{ab} , respectively. We describe the detail in Appendix B. The equation for $\Phi(0, r)$ is the same as that in the Brill-Lindquist case [6] and the solution is given by

$$\Phi(0, r) = (z_0^2) \frac{n}{4(n^2 - 1)K_2^{[n]}} \frac{\sqrt{r} [n^2 + 3n + 4 + n(n+3)\sqrt{f}]}{H(r)R^{(n+3)/2}}, \quad (54)$$

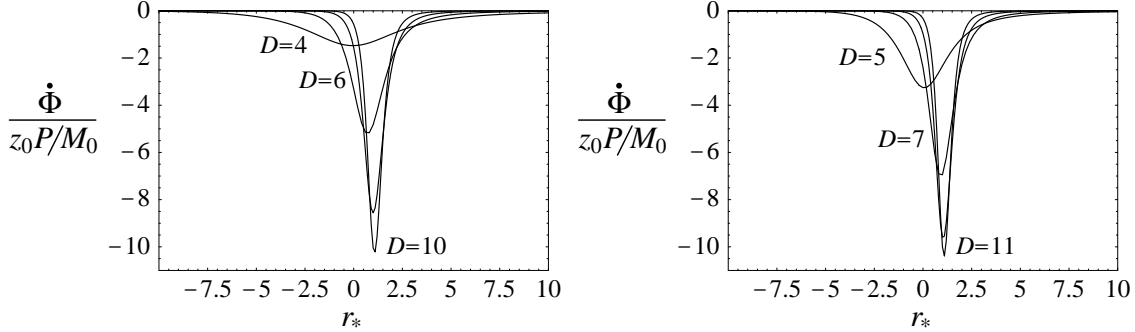


FIG. 4: Time derivative of the master variable $\dot{\Phi}$ in the unit of $z_0 P/M_0$ for $D \equiv n + 2 = 4, 6, 8, 10$ (left) and for $D = 5, 7, 9, 11$ (right). For $P > 0$, $\dot{\Phi}$ is negative.

where the definition of $K_2^{[n]}$ is given in Eq. (B3). This has the order of z_0^2 . On the other hand, $\dot{\Phi}(0, r)$ is proportional to $z_0 P/M_0$ and its value is obtained by solving Eq. (B27) described in Appendix B. The solution is

$$\dot{\Phi}(0, r) = -(z_0 P/M_0) \frac{2n}{(n-1)K_2^{[n]}} \frac{\sqrt{f}}{r^{n/2+1}} \frac{2(n+2) + (n+1)x}{2(n+2) + n(n+1)x}. \quad (55)$$

We show the behavior of $\dot{\Phi}(0, r_*)$ in Fig. 4.

Since Eq. (48) is linear, Φ is naturally decomposed into two parts

$$\Phi = (z_0^2) \widehat{\Phi}_{\text{BL}} + (z_0 P/M_0) \widehat{\Phi}_{\text{BY}}. \quad (56)$$

The solution for $\widehat{\Phi}_{\text{BL}}$ is the same as that in the time-symmetric case derived in our previous paper [6]³. Here, we show only the computation of $\widehat{\Phi}_{\text{BY}}$. For the numerical computation, we use the second-order finite differencing code developed in [6] and solve the equation in the domain $-200 \leq r_* \leq 1000$ with the grid spacings $dr_* = 0.01$ ($D = 4-7$) and 0.005 ($D = 8-11$) and $dt = 0.2dr_*$. Computation was performed changing the grid spacing and we confirmed that the numerical results converge at second order. For the chosen grid spacing, the error evaluated with ϵ_1 in Eq. (31) is 0.05%–0.9% for $D = 4-7$ and 0.4%–2% for $D = 8-11$. The error in the values listed in Table II is $\lesssim 0.1\%$.

³ In [6], $\Phi(0, r_*)$ was solved numerically. We recalculated the temporal evolution using the analytic formula (54) of the initial condition and found that the difference between the two is $\sim 10^{-5}\%$.

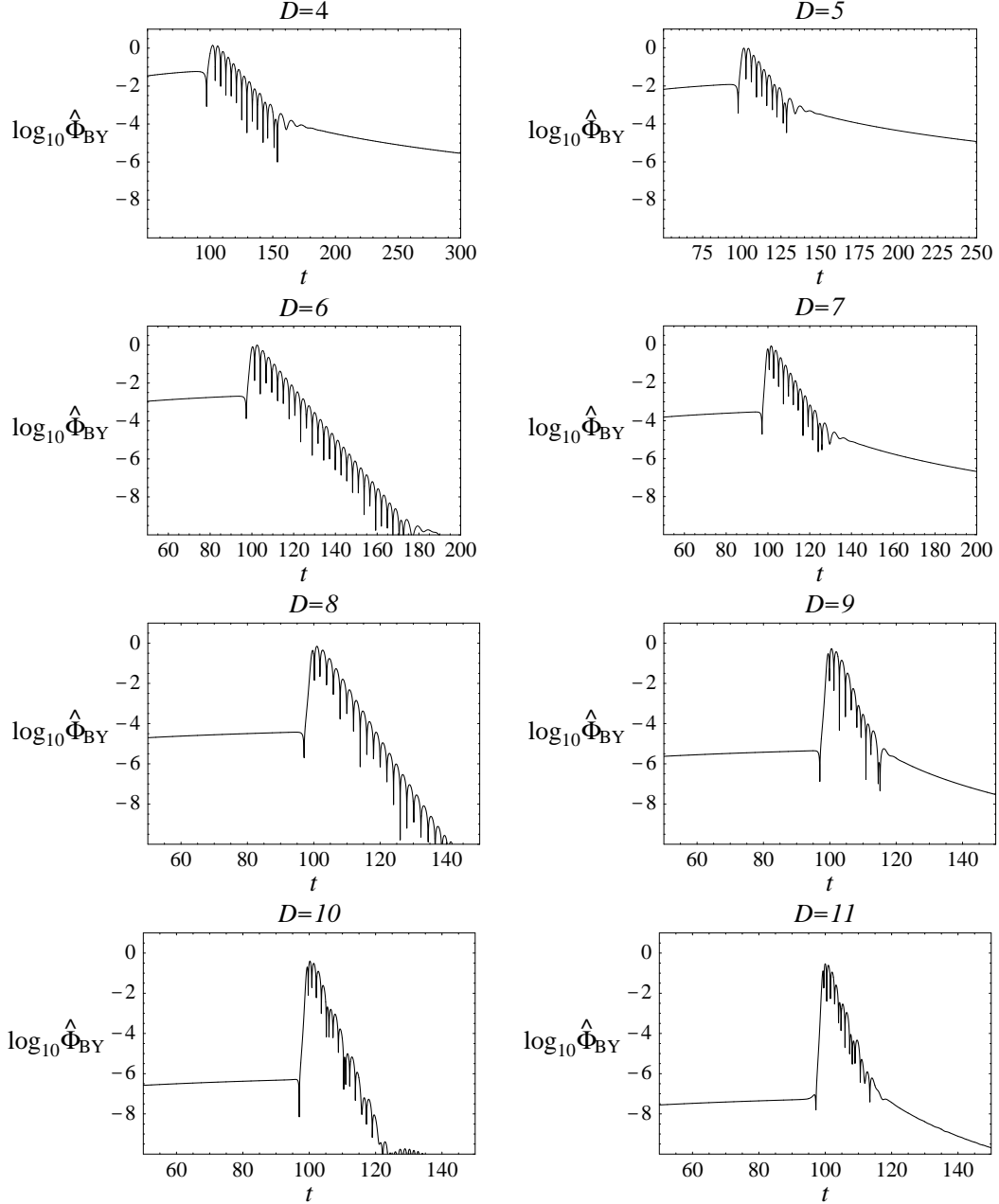


FIG. 5: The time evolution of $\hat{\Phi}_{\text{BY}}$ for $D = 4-11$ observed at $r_* = 100$.

C. Numerical results

Figure 5 shows numerical results for the time evolution of $\hat{\Phi}_{\text{BY}}$. Soon after the onset of the calculation, a quasi-normal mode is excited irrespective of dimension and, subsequently, the power-law tail is seen for four and odd dimensions. We read off the quasinormal frequencies ω_{QN} and checked the consistency with previous results of ω_{QN} listed in [6, 13, 14]. The

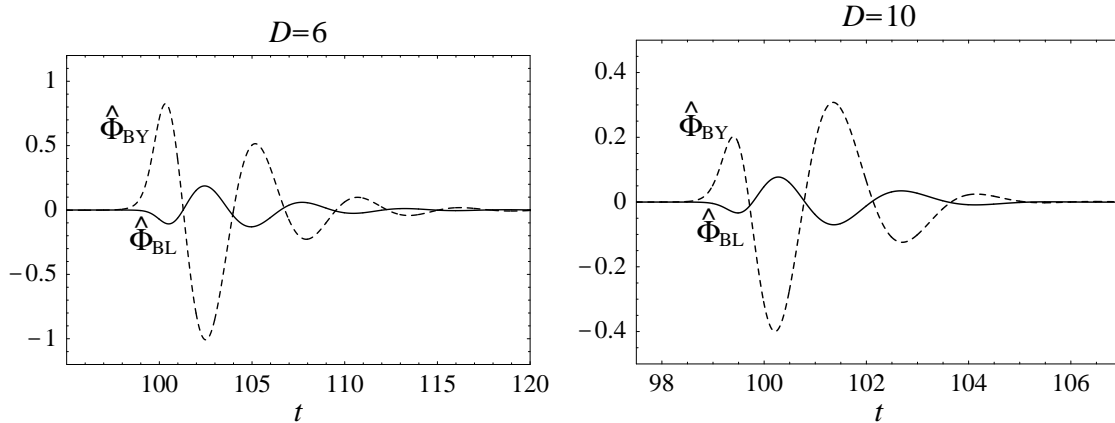


FIG. 6: The time evolution of $\hat{\Phi}_{\text{BY}}$ (dashed line) and $\hat{\Phi}_{\text{BL}}$ (solid line) for $D = 6$ (left) and 10 (right) observed at $r_* = 100$.

TABLE II: The values of c_1 , c_2 and c_3 of Eq. (58) for $D = 4$ –11.

D	4	5	6	7	8	9	10	11
c_1	0.0252	0.0245	0.0290	0.0288	0.0258	0.0223	0.0194	0.0172
c_2	-0.165	-0.243	-0.294	-0.287	-0.251	-0.213	-0.182	-0.158
c_3	0.343	0.671	0.808	0.765	0.647	0.539	0.456	0.396

behaviors of $\hat{\Phi}_{\text{BL}}$ and $\hat{\Phi}_{\text{BY}}$ are compared in Fig. 6 for $D = 6$ and 10. It is found that phases of $\hat{\Phi}_{\text{BL}}$ and $\hat{\Phi}_{\text{BY}}$ disagree and the phase shift is $\approx \pi$. This implies that two terms interfere each other. This feature universally holds irrespective of the dimensionality.

From $\hat{\Phi}_{\text{BL}}$ and $\hat{\Phi}_{\text{BY}}$, we calculate the radiated energy of gravitational waves by the following formula (see [6, 14] for a derivation):

$$E_{\text{rad}} = \frac{k^2(n-1)(k^2-n)}{32\pi nG} \int \dot{\Phi}^2 dt. \quad (57)$$

Substituting Eq. (56) into the above formula, E_{rad} is rewritten as

$$\frac{E_{\text{rad}}}{M_0} = c_1 z_0^4 + c_2 z_0^3 (P/M_0) + c_3 z_0^2 (P/M_0)^2, \quad (58)$$

where c_1 , c_2 , and c_3 are constants determined by numerical integration. These values are listed in Table II. The formula (58) together with Table II will be used for the benchmark of the fully nonlinear analysis in numerical relativity as in the four-dimensional case [8, 9].

Figure 7 shows the contours of E_{rad}/M_0 on the $(z_0/R_h(M_0), P/M_0)$ -plane. For a fixed value of z_0 , the radiated energy decreases as the value of P/M_0 is increased for small values

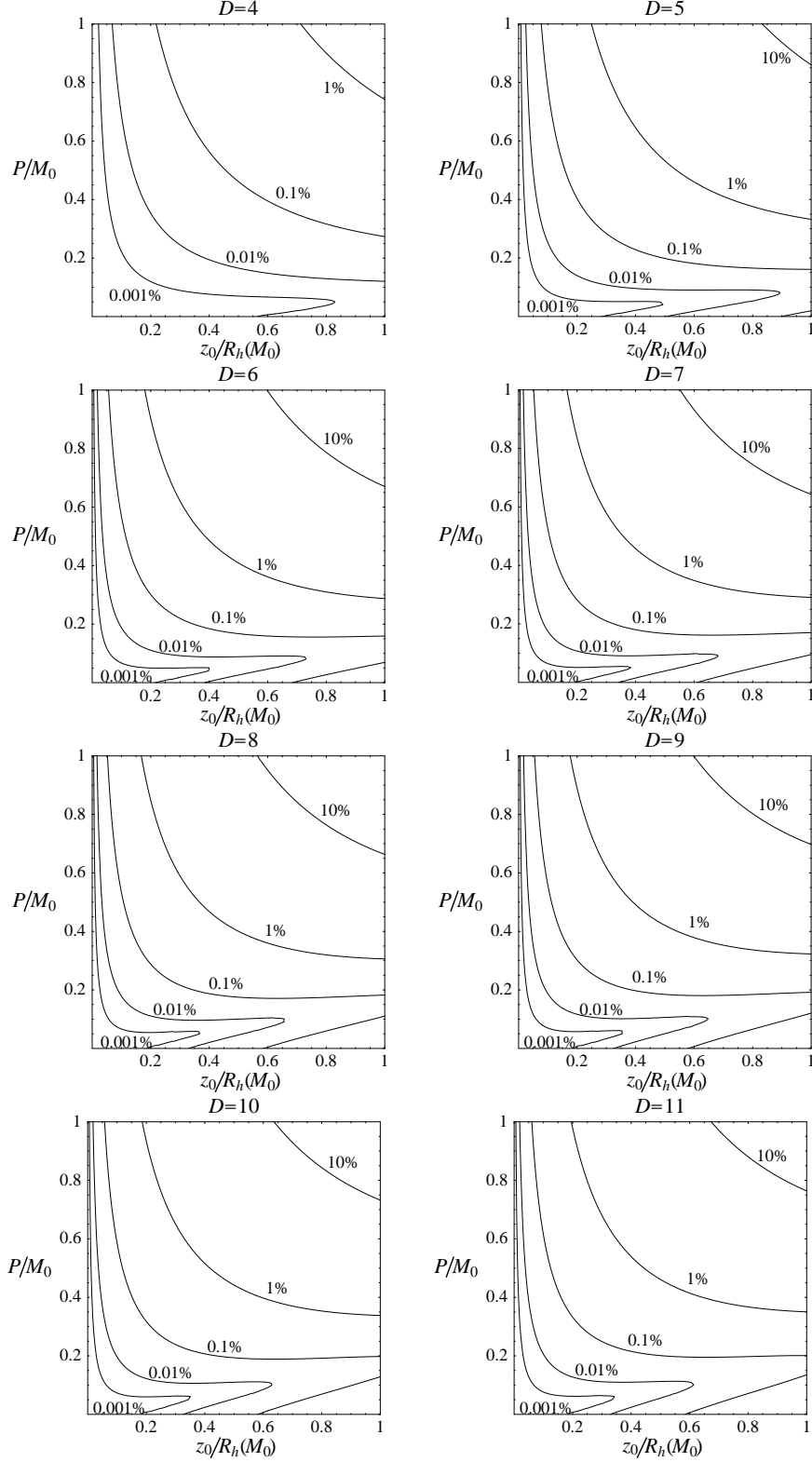


FIG. 7: Contours of radiation efficiency E_{rad}/M_0 (shown in the unit of %) on the $(z_0/R_h(M_0), P/M_0)$ -plane for $D = 4-11$ predicted by the close-slow analysis. Note that the unit of z_0 is $R_h(M_0)$ in this figure.

TABLE III: The values of E_{rad}/M_0 evaluated on the AH critical line for $P/M_0 = 0.0, 0.5, 1.0$. The unit is %.

D	4	5	6	7	8	9	10	11
$P/M_0 = 0.0$	0.0034	0.059	0.20	0.34	0.44	0.49	0.51	0.52
$P/M_0 = 0.5$	0.30	1.76	2.83	3.01	2.80	2.53	2.28	2.08
$P/M_0 = 1.0$	1.6	7.3	11.5	12.2	12.0	11.4	10.5	9.8

of P as $P/M_0 \lesssim 0.2 \times z_0$. This is because the phases of $\widehat{\Phi}_{\text{BL}}$ and $\widehat{\Phi}_{\text{BY}}$ disagree by a factor of $\approx \pi$ (cf. Fig. 6). In the range $P/M_0 \gtrsim 0.2 \times z_0$, the amplitude of second term in Eq. (56) exceeds the first term and E_{rad} increases as P/M_0 is increased. The similar behavior was reported in the four dimension case [9].

D. Dependence on dimensionality

To get some insight for the dependence of radiation efficiency on the value of D , we evaluate E_{rad}/M_0 by choosing characteristic values of z_0 and P for $D = 4-11$. In comparison, we fix the value of P/M_0 since $P/2M_0$ could be interpreted as the value of momentum divided by the rest mass, i.e., $v/\sqrt{1-v^2}$ where v is the velocity of each incoming black hole. We adopt $P/M_0 = 0, 0.5$ and 1 which corresponds to $\gamma = 1$, $\sqrt{2} \simeq 1.41$, and $\sqrt{5} \simeq 2.24$. Then we recall Fig. 2 and evaluate E_{rad} on the AH critical line, since the close-slow approximation holds for the system sufficiently close to the Schwarzschild spacetime and it is necessary to choose z_0 for which the common AH presents.

Table III shows the values of E_{rad}/M_0 evaluated in this procedure. In the higher-dimensional cases, it is $\sim 2\%-3\%$ for $P/M_0 = 0.5$ and $\sim 10\%$ for $P/M_0 = 1.0$. These values do not depend significantly on D in the higher-dimensional cases. Note that the values in Table III does not contradict the bounds derived from the AH area shown in Table I.

The difference between M_0 and M_{ADM} increases with increase of P/M_0 (cf. Fig. 1). This difference comes from time asymmetry of the initial data and has the magnitude of order $(z_0 P/M_0)^2$. Thus for a large difference with $M_{\text{ADM}}/M_0 - 1 \gtrsim 0.1$, the linear approximation breaks down. In the four-dimensional case, we know that the nonlinear effect suppresses

$E_{\text{rad}}/M_{\text{ADM}}$ [9]. If this is also the case for $D \geq 5$, the value of $E_{\text{rad}}/M_{\text{ADM}} \sim 10\%$ for P/M_0 would be an overestimate and would indicate that gravitational radiation do not significantly contribute to the loss of the system energy in the head-on collision of two black holes.

V. DISCUSSION

In this paper, we presented a generalized Bowen-York formulation for the initial value problem of multi-black holes in higher-dimensional space. Using this formulation, we derived analytic solutions of the momentum constraint equation for extrinsic curvature of moving black holes in the conformally flat higher-dimensional space. As an application, initial data for head-on collision of two equal-mass black holes were computed numerically solving the Hamiltonian constraint for the conformal factor. The properties of the obtained space such as the ADM mass and the common AH were analyzed. We determined the critical line for formation of a common AH in the parameter space of (z_0, P) .

Then, we evolved this system using the close-slow approximation and analyzed gravitational waves. We derived the formula for the radiated energy for a wide variety of D [see Eq. (58) together with Table II] and clarified that it depends weakly on D ; irrespective of D the efficiency is less than $\sim 10\%$ for $P/M_0 \leq 1$ and $z_0 \leq r_h(M_0)$.

As we mentioned in Sec. I, one of the motivations of this study is to clarify the total radiated energy of gravitational waves in the black hole formation through particle collisions in accelerators. However, there are two shortcomings in this study. One is that we use the linear perturbation method which provides a reliable result only for small values of z_0 and P . The other is that the Bowen-York black holes system does not accurately model the high-energy particles system.

As for the first problem, we can learn from the four-dimensional study. In [9], the results of the close-slow approximation and of the fully nonlinear numerical simulation are compared. It shows that the results in the close-slow approximation agrees approximately with the fully nonlinear results for small separation and small momentum. However, the difference becomes larger as separation or momentum is increased. For $P \gg M_0$, the nonlinear numerical results indicate that the radiation efficiency increases as P is increased and approaches to an asymptotic value, while extrapolation of the linear perturbation results gives infinity. To know the results for $P \gg M_0$ in higher-dimensional spacetime, obviously, fully nonlinear

numerical simulation is necessary.

The difference between the high-energy particles and the Bowen-York black holes is the other problem. As the model of a high-energy particle, the metric of Aichelburg-Sexl [15] is often used. It is obtained by boosting the Schwarzschild black hole to the speed of light with fixed energy $p = \gamma m$ and taking lightlike limit $\gamma \rightarrow \infty$. The gravitational field is localized in the transverse plane to the direction of motion and forms a gravitational shock wave, which is a reminiscent of the infinite Lorentz contraction of the isotropic gravitational field of the original Schwarzschild black hole. The spacetime is flat except at the shock wave and this enables us to write down the metric of two high-energy particles outside of the lightcone of shock collision. Hence, the AH formation at the instant of collision has been investigated so far [16, 17, 18].

Obviously, gravitational field (the conformal factor or the extrinsic curvature) is not localized in the case of Bowen-York black holes. This indicates that the Bowen-York black holes system cannot be a precise model for the high-energy particles system even in the case $z_0 \gg R_h(M_0)$ and $P \gg M_0$. Actually, there exist several discussions [19] about the fact that the Bowen-York black hole system contains unphysical gravitational waves, i.e., so-called junk energy. Thus, in the fully nonlinear numerical calculation with the Bowen-York initial data, one should take into account the possibility that junk energy changes the estimate of radiation efficiency. To avoid this, one should make the junk energy radiate away before the collision setting the initial separation sufficiently large.

Finally, we comment on the importance of the study of the grazing collision. In the head-on collision case, the upper bound on the radiation efficiency ($\lesssim 40\%$) in the head-on collision of Aichelburg-Sexl particles was obtained [16] by studying the AH area and applying the area theorem. Although the same discussion was done in the grazing collision with nonzero impact parameter b [17, 18], the upper bound on the radiation efficiency is very weak for large b . Hence, the direct calculation of gravitational radiation in the grazing collision is more important than the head-on collision case. Also, it is required to calculate the Kerr parameter of the resultant black hole. In order to solve these problems, the off-axis collision of the Bowen-York black holes could be an approximation and provide several implications. We plan to study this process using the close-slow approximation as a first step.

Acknowledgments

The work of H. Y. was partially supported by a Grant for The 21st Century COE Program (Holistic Research and Education Center for Physics Self-Organization Systems) at Waseda University. H. Y. also thanks the Killam Trust for the financial support. The work of T. S. was supported by Grant-in-Aid for Scientific Research from Ministry of Education, Science, Sports and Culture of Japan (No. 13135208, No. 14102004, No. 17740136 and No. 17340075), the Japan-U.K. and Japan-France Research Cooperative Program.

APPENDIX A: OTHER SOLUTIONS OF EXTRINSIC CURVATURE

We briefly comment on other solutions of $\widehat{K}_{\mu\nu}$ for the momentum constraint (7), which were not introduced in Sec. II. Since the equations for B_μ and χ are pure Laplace equations, we can make infinite number of solutions for the extrinsic curvature. Here, we present solution of low-multipole momenta.

To make a spinning black hole, we write

$$B_\mu = \frac{(n-1)\pi G J_{\mu\nu} n^\nu}{n\Omega_n R^n}, \quad \chi = 0 \quad (\text{A1})$$

where $J_{\mu\nu}$ is an anti-symmetric tensor. Then, $\widehat{K}_{\mu\nu}$ is written as

$$\widehat{K}_{\mu\nu} = -\frac{4\pi(n+1)G}{\Omega_n R^{n+1}} (J_{\mu\rho} n^\rho n_\nu + J_{\nu\rho} n^\rho n_\mu). \quad (\text{A2})$$

$J_{\mu\nu}$ denotes an angular momentum tensor expressed by

$$J_{\mu\nu} = \frac{1}{8\pi G} \int_{R \rightarrow \infty} (x_\mu K_{\nu\rho} - x_\nu K_{\mu\rho}) n^\rho dS. \quad (\text{A3})$$

In the three-dimensional case, we can define the angular momentum vector by the formula

$$J_\mu = \frac{1}{2} \epsilon_{\mu\nu\rho} J^{\nu\rho}. \quad (\text{A4})$$

The conformal factor Ψ can be determined by solving the Hamiltonian constraint in the same procedure as in Sec. III.

It is possible to derive other solutions, e.g., by setting

$$B_\mu = \frac{C_{\mu\nu} n^\nu}{R^n}, \quad \chi = 0, \quad (\text{A5})$$

or

$$B_\mu = \frac{C_{\mu\nu\rho}}{R^{n+1}} \left[n_\nu n_\rho - \frac{\delta_{\nu\rho}}{(n+1)} \right], \quad \chi = 0, \quad (\text{A6})$$

where $C_{\mu\nu}$ and $C_{\mu\nu\rho}$ are symmetric and anti-symmetric tensors, respectively. However the physical meaning of these solutions is unclear.

APPENDIX B: INITIAL CONDITION OF THE MASTER VARIABLE

In this appendix, we explain how to set the initial condition of the master variable Φ . We begin by studying the initial condition of the following perturbative metric

$$\delta h_{\mu\nu} = \begin{pmatrix} fH_0\mathbb{S} & H_1\mathbb{S} & h_0\mathbb{S}_\theta & h_0\mathbb{S}_{\phi_*} \\ \text{sym.} & f^{-1}H_2\mathbb{S} & h_1\mathbb{S}_\theta & h_1\mathbb{S}_{\phi_*} \\ \text{sym.} & \text{sym.} & 2r^2(H_L\gamma_{\theta\theta}\mathbb{S} + H_T\mathbb{S}_{\theta\theta}) & 2r^2(H_L\gamma_{\theta\phi_*}\mathbb{S} + H_T\mathbb{S}_{\theta\phi_*}) \\ \text{sym.} & \text{sym.} & \text{sym.} & 2r^2(H_L\gamma_{\phi_*\phi_*}\mathbb{S} + H_T\mathbb{S}_{\phi_*\phi_*}) \end{pmatrix} \quad (\text{B1})$$

where \mathbb{S} denotes the hyper-spherical harmonics

$$\mathbb{S} = S_\ell^{[n]} \equiv K_\ell^{[n]} C_\ell^{[(n-1)/2]}(\cos\theta), \quad (\text{B2})$$

$$K_\ell^{[n]} = \left[\frac{4\pi^{(n+1)/2}\Gamma(n+\ell-1)}{(n+2\ell-1)\Gamma(\ell+1)\Gamma((n-1)/2)\Gamma(n-1)} \right]^{-1/2}, \quad (\text{B3})$$

on the unit sphere of which metric is

$$\gamma_{ij}dz^i dz^j = d\theta^2 + \sin^2\theta d\Omega_{n-1}^2. \quad (\text{B4})$$

\mathbb{S}_i and \mathbb{S}_{ij} are given by

$$\mathbb{S}_i = -\frac{1}{k}\widehat{D}_i\mathbb{S}, \quad (\text{B5})$$

$$\mathbb{S}_{ij} = \frac{1}{k^2}\widehat{D}_i\widehat{D}_j\mathbb{S} + \frac{1}{n}\gamma_{ij}\mathbb{S}, \quad (\text{B6})$$

where \widehat{D}_i denotes the covariant derivative on the unit sphere and k is defined in Eq. (51). Since the initial metric is the Brill-Lindquist one, the values of H_2, H_L, H_T, h_1 are same as the ones that we have derived in [6]:

$$H_2 = 2H_L = \chi(r) \equiv \frac{1/(n-1)R^{n-1}}{1+1/4R^{n-1}} \left(\frac{z_0}{R}\right)^2 \left(K_2^{[n]}\right)^{-1}, \quad (\text{B7})$$

$$h_1 = H_T = 0. \quad (\text{B8})$$

Here our purpose is to compute the time derivative of these variables.

The nonzero components of $\widehat{K}_{\mu\nu}$ shown in Eqs. (40)–(42) are rewritten as

$$\widehat{K}_{RR} = -(z_0 P/M_0) \left[(n+2) \frac{S_2^{[n]}}{K_2^{[n]}} + n \frac{S_0^{[n]}}{K_0^{[n]}} \right] R^{-(n+1)}, \quad (\text{B9})$$

$$\widehat{K}_{ij} = (z_0 P/M_0) \left[\frac{n+2}{n} \frac{S_2^{[n]}}{K_2^{[n]}} \gamma_{ij} + \frac{2(n+1)}{n-1} \frac{S_2^{[n]}{}_{ij}}{K_2^{[n]}} + \frac{S_0^{[n]}}{K_0^{[n]}} \gamma_{ij} \right] R^{-(n-1)}. \quad (\text{B10})$$

Thus $K_{\mu\nu}$ is composed of $\ell = 0$ and 2 modes. Since $\ell = 0$ mode is absorbed in a coordinate transformation, we omit it hereafter. The extrinsic curvature $K_{\mu\nu} = \Psi^{-2} \widehat{K}_{\mu\nu} \simeq \Psi_0^{-2} \widehat{K}_{\mu\nu}$ [where Ψ_0 is defined in Eq. (44)] in the (r, θ, ϕ_*) coordinate is

$$K_{rr} = -(z_0 P/M_0) \left[(n+2) \frac{S_2^{[n]}}{K_2^{[n]}} \right] f^{-1} \Psi_0^{-2(n+1)/(n-1)} R^{-(n+1)}. \quad (\text{B11})$$

$$K_{ij} = (z_0 P/M_0) \left[\frac{n+2}{n} \frac{S_2^{[n]}}{K_2^{[n]}} \gamma_{ij} + \frac{2(n+1)}{n-1} \frac{S_2^{[n]}{}_{ij}}{K_2^{[n]}} \right] \Psi_0^{-2} R^{-(n-1)}. \quad (\text{B12})$$

$K_{\mu\nu}$ is written as

$$K_{\mu\nu} = -\frac{1}{2\alpha} \left(\dot{h}_{\mu\nu} - \nabla_\mu \beta_\nu - \nabla_\nu \beta_\mu \right) \quad (\text{B13})$$

in terms of the lapse function $\alpha = \sqrt{f}$ and the shift vector β_μ . Although β_μ can be freely chosen provided that $O(\beta_\mu) = O(z_0^2)$, we impose $\beta_\mu = 0$ for simplicity. This brings us $H_1 = h_0 = 0$ and $\dot{h}_{\mu\nu} = -2\sqrt{f} K_{\mu\nu}$. Using Eqs. (B11) and (B12), we have the explicit formulas of \dot{h}_{rr} and \dot{h}_{ij} and they are compared with Eq. (B1):

$$\dot{h}_1 = 0, \quad (\text{B14})$$

$$\dot{H}_2 = 2(n+2)\eta(r), \quad (\text{B15})$$

$$\dot{H}_L = -\frac{n+2}{n}\eta(r), \quad (\text{B16})$$

$$\dot{H}_T = -\frac{2(n+1)}{n-1}\eta(r), \quad (\text{B17})$$

where

$$\eta(r) = \frac{(z_0 P/M_0) \sqrt{f}}{K_2^{[n]} r^{n+1}}. \quad (\text{B18})$$

Now we are in a position to derive the equation for Φ and $\dot{\Phi}$. Setting

$$f_{ab} = \begin{pmatrix} fH_0 & H_1 \\ H_1 & H_2/f \end{pmatrix}, \quad r f_a = (h_0, h_1), \quad (\text{B19})$$

the gauge invariant quantities derived in [12] are

$$F = H_L + (1/n)H_T + (1/r)D^a r X_a, \quad (\text{B20})$$

$$F_{ab} = f_{ab} + D_a X_b + D_b X_a, \quad (\text{B21})$$

where

$$X_a = \frac{r}{k} \left(f_a + \frac{r}{k} D_a H_T \right), \quad (\text{B22})$$

and D_a denotes the covariant derivative with respect to the metric $g_{ab} dy^a dy^b = -f dt^2 + f^{-1} dr^2$. In our case,

$$X_t = \frac{r^2}{k^2} \dot{H}_T, \quad X_r = 0, \quad (\text{B23})$$

and

$$F = \chi(r)/2. \quad (\text{B24})$$

F is related to Φ and $\Phi_{,r}$ as shown in [12] and we find the same equation for Φ as that in our previous paper [6]. Hence, the initial value of Φ is unchanged. Calculating F_{rt} , we obtain

$$F_{rt} = -\frac{2(n+1)}{n-1} \frac{r^2}{k^2} \left[\left(\frac{2}{r} - \frac{f_{,r}}{f} \right) \eta(r) + 2\eta_{,r}(r) \right], \quad (\text{B25})$$

where we have substituted Eq. (B17). Since F_{rt} is related to $\dot{\Phi}$ and $\dot{\Phi}_{,r}$ as

$$F_{rt} = r^{1-n/2} \left(-\frac{P_Z}{4Hf} \dot{\Phi} + r \dot{\Phi}_{,r} \right), \quad (\text{B26})$$

we find the equation

$$\dot{\Phi}_{,r} = \frac{P_Z}{4Hrf} \dot{\Phi} + \frac{2n}{n-1} r^{n/2-1} \eta(r), \quad (\text{B27})$$

where P_Z is a function of r given in [12] and we used Eq. (B18). The solution is given by Eq. (55).

- [1] N. Arkani-Hamed, S. Dimopoulos and G. R. Dvali, Phys. Lett. B **429**, 263 (1998) [arXiv:hep-ph/9803315];
I. Antoniadis, N. Arkani-Hamed, S. Dimopoulos and G. R. Dvali, *ibid.* **436**, 257 (1998) [arXiv:hep-ph/9804398];
- [2] L. Randall and R. Sundrum, Phys. Rev. Lett. **83**, 3370 (1999) [arXiv:hep-ph/9905221].
- [3] L. Randall and R. Sundrum, Phys. Rev. Lett. **83**, 4690 (1999) [arXiv:hep-th/9906064].

- [4] T. Banks and W. Fischler, arXiv:hep-th/9906038.
 S. B. Giddings and S. Thomas, Phys. Rev. D **65**, 056010 (2002) [arXiv:hep-ph/0106219];
 S. Dimopoulos and G. Landsberg, Phys. Rev. Lett. **87**, 161602 (2001) [arXiv:hep-ph/0106295],
- [5] G. Landsberg, arXiv:hep-ph/0211043;
 M. Cavaglia, Int. J. Mod. Phys. A **18**, 1843 (2003) [arXiv:hep-ph/0210296];
 P. Kanti, Int. J. Mod. Phys. A **19**, 4899 (2004) [arXiv:hep-ph/0402168];
 S. Hossenfelder, arXiv:hep-ph/0412265.
- [6] H. Yoshino, T. Shiromizu and M. Shibata, Phys. Rev. D **72**, 084020 (2005) [arXiv:gr-qc/0508063].
- [7] J. M. Bowen and J. W. York, Jr, Phys. Rev. D **21**, 2047 (1980).
- [8] R. H. Price and J. Pullin, Phys. Rev. Lett. **72**, 3297 (1994) [arXiv:gr-qc/9402039].
- [9] J. Baker, A. Abrahams, P. Anninos, S. Brandt, R. Price, J. Pullin and E. Seidel, Phys. Rev. D **55**, 829 (1997) [arXiv:gr-qc/9608064].
- [10] F. Pretorius, Phys. Rev. Lett. **95**, 121101 (2005) [arXiv:gr-qc/0507014];
 M. Campanelli, C. O. Lousto, P. Marronetti and Y. Zlochower, Phys. Rev. Lett. **96**, 111101 (2006) [arXiv:gr-qc/0511048].
 J. G. Baker, J. Centrella, D. I. Choi, M. Koppitz and J. van Meter, Phys. Rev. Lett. **96**, 111102 (2006) [arXiv:gr-qc/0511103];
 P. Diener *et al.*, Phys. Rev. Lett. **96**, 121101 (2006) [arXiv:gr-qc/0512108];
 F. Herrmann, D. Shoemaker and P. Laguna, arXiv:gr-qc/0601026.
- [11] S. Brandt and B. Bruggmann, Phys. Rev. Lett. **78**, 3606 (1997) [arXiv:gr-qc/9703066].
- [12] H. Kodama and A. Ishibashi, Prog. Theor. Phys. **110**, 701 (2003) [arXiv:hep-th/0305147].
- [13] R. A. Konoplya, Phys. Rev. D **68**, 024018 (2003) [arXiv:gr-qc/0303052];
 R. A. Konoplya, Phys. Rev. D **68**, 124017 (2003) [arXiv:hep-th/0309030].
- [14] E. Berti, M. Cavaglia and L. Gualtieri, Phys. Rev. D **69**, 124011 (2004) [arXiv:hep-th/0309203].
- [15] P. C. Aichelburg and R. U. Sexl, Gen. Rel. Grav. **2**, 303 (1971).
- [16] D. M. Eardley and S. B. Giddings, Phys. Rev. D **66**, 044011 (2002), [arXiv:gr-qc/0201034];
- [17] H. Yoshino and Y. Nambu, Phys. Rev. D **67**, 024009 (2003) [arXiv:gr-qc/0209003];
- [18] H. Yoshino and V. S. Rychkov, Phys. Rev. D **71**, 104028 (2005) [arXiv:hep-th/0503171].
- [19] N. Jansen, P. Diener, A. Khokhlov and I. Novikov, Class. Quant. Grav. **20**, 51 (2003)

[arXiv:gr-qc/0103109].